

Characterization of the diffraction efficiency of polymer-liquid-crystal-polymer-slices gratings at all incidence angles

Man Xu¹, Luciano De Sio², Roberto Caputo², Cesare P. Umeton², Arthur J. H. Wachters³, Dick K. G. de Boer³ and H. Paul Urbach¹

¹ Optics Research Group, Delft University of Technology,
Lorentzweg 1, 2628 CJ Delft, the Netherlands

² LICRYL (Liquid Crystals Laboratory), National Institute for the Physics of Matter (INFN-CNR), Center of Excellence CEMIF.CAL and Department of Physics, University of Calabria, 87036 Arcavacata di Rende (CS), Italy

³ Philips Research Laboratory, High Tech Campus 34, 5656 AE Eindhoven, The Netherlands
m.xu@tudelft.nl

Abstract: Recently, a novel holographic diffraction grating made of polymer slices alternated to homogeneous films of nematic liquid crystal (POLICRYPS) was realized. We study the optical performance of the POLICRYPS gratings by both numerical simulations and experiments. Characterization of the grating at normal and conical reading mount are performed. The diffraction efficiency depends strongly on the angles of incidence. Besides, the characterization of the diffraction efficiency at Bragg angle incidence is studied. A uniform high diffraction efficiency is achieved when the incident wave satisfies the Bragg condition.

© 2008 Optical Society of America

OCIS codes: (050.1950) Diffraction gratings; (050.7330) Volume gratings; (090.2890) Holographic optical elements; (160.3710) Liquid crystals.

References and links

1. J. Margerum, A. Lackner, E. Ramos, G. Smith, N. Vaz, J. Kohler, and C. Allison, "Polymer dispersed liquid crystal film devices," U.S. Patent (1992).
2. R. L. Sutherland, V. P. Tondiglia, L. V. Natatajan, T. J. Bunning, and W. W. Adams, "Electro-Optical Switching Characteristics of Volume Holograms in Polymer Dispersed Liquid Crystals," *J. Nonlinear Opt. Phys. Mater.* **5**(1), 89 (1996).
3. D. E. Lucchetta, R. Karapinar, A. Manni, , and F. Simoni, "Phase-only modulation by nanosized polymer-dispersed liquid crystals," *J. Appl. Phys.* **91**(9), 6060 – 6065 (2002).
4. R. Caputo, L. De Sio, A. Veltri, C. Umeton, and A. V. Sukhov, "Development of a new kind of switchable holographic grating made of liquid-crystal films separated by slices of polymeric material," *Opt. Lett.* **29**(11), 1261 – 1263 (2004). URL <http://www.opticsinfobase.org/abstract.cfm?URI=jdt-2-1-38>.
5. L. De Sio, R. Caputo, A. De Luca, A. Veltri, C. Umeton, and A. V. Sukhov, "In situ optical control and stabilization of the curing process of holographic gratings with a nematic film-polymer-slice sequence structure," *Appl. Opt.* **45**(16), 3721 – 3727 (2006). URL <http://www.opticsinfobase.org/abstract.cfm?URI=ao-45-16-3721>.
6. R. Caputo, A. V. Sukhov, C. P. Umeton, and R. F. Ushakov, "Formation of a grating of submicron nematic layers by photopolymerization of nematic-containing mixtures," *J. Exp. Theor. Phys.* **91**(6), 1190–1197 (2000).
7. R. Caputo, L. De Sio, A. Veltri, C. P. Umeton, and A. V. Sukhov, "POLICRYPS switchable holographic grating: a promising grating electro-optical pixel for high resolution display application," *J. Display Technology*, **2**(1), 38–51 (2006).

8. H. Kogelnik, "Coupled wave theory for thick hologram gratings," *Bell Syst. Tech. J.* **48**(9), 2909–2947 (1969). URL <http://adsabs.harvard.edu/abs/1969BSTJ...48.2909K>.
9. K. Rokushima and J. Yamakita, "Analysis of anisotropic dielectric gratings," *J. Opt. Soc. Am. A* **73**, 901 (1983).
10. E. N. Glytsis and T. K. Gaylord, "Rigorous three-dimensional coupled-wave diffraction analysis of single and cascaded anisotropic gratings," *J. Opt. Soc. Am. A* **4**, 2061 (1987).
11. S. Mori, K. Mukai, J. Yamakita, and K. Rokushima, "Analysis of dielectric lamellar gratings coated with anisotropic layers," *J. Opt. Soc. Am. A* **7**, 1661 (1990).
12. G. Montemezzani and M. Zgonik, "Light diffraction at mixed phase and absorption gratings in anisotropic media for arbitrary geometries," *Phys. Rev. E* **55**(1), 1035 – 1047 (1997). URL <http://link.aps.org/abstract/PRE/v55/p1035>.
13. J. B. Harris, T. W. Preist, E. L. Wood, and J. R. Sambles, "Conical diffraction from multicoated gratings containing uniaxial materials," *J. Opt. Soc. Am. A* **13**, 803 (1996).
14. L. Li, "Reformulation of the Fourier modal method for surface-relief gratings made with anisotropic materials," *J. Mod. Opt.* **45**, 1313 (1998).
15. X. Wei, "Three Dimensional Rigorous Model for Optical Scattering Problems," Ph.D. thesis, Delft University of Technology, Lorentzweg 1, 2628 CJ Delft (2006). URL <http://www.optica.tn.tudelft.nl/publications/summary/wei.asp>.
16. X. Wei, A. J. Wachtters, and H. P. Urbach, "Finite-element model for three-dimensional optical scattering problems," *J. Opt. Soc. Am. A* **24**(3), 866–881 (2007). URL <http://www.opticsinfobase.org/abstract.cfm?URI=josaa-24-3-866>.
17. Norland, "Norland Optical Adhesive 61," URL <http://www.norlandprod.com/adhesives/noa61pg2.html>.
18. A. Veltri, R. Caputo, C. Umton, and A. V. Sukhov, "Model for the photoinduced formation of diffraction gratings in liquid-crystalline composite materials," *Appl. Phys. Lett.* **84**(18), 3492–3494 (2004). URL <http://link.aip.org/link/?APPLAB/84/3492/1>.
19. M. Xu, H. P. Urbach, and D. K. G. de Boer, "Simulations of birefringent gratings as polarizing color separator in backlight for flat-panel displays," *Opt. Express* **15**(9), 5789–5800 (2007). URL <http://www.opticsinfobase.org/abstract.cfm?URI=oe-15-9-5789>.
20. URL <http://www.math.tu-berlin.de/ilupack/>.
21. O. Schenk and K. Gärtner, "Solving Unsymmetric Sparse Systems of Linear Equations with PARDISO," *J. Future Generation Computer Systems* **20**, 475–487 (2004).
22. O. Schenk and K. Gärtner, "On fast factorization pivoting methods for symmetric indefinite systems," *Elec. Trans. Numer. Anal.* **23**, 158–179 (2006).
23. R. Caputo, L. De Sio, M. J. J. Jak, E. J. Hornix, D. K. G. de Boer, , and H. J. Cornelissen, "Short period holographic structures for backlight display applications," *Opt. Express* **15**(17), 10,540 – 10,552 (2007). URL <http://www.opticsinfobase.org/abstract.cfm?URI=oe-15-17-10540>.

1. Introduction

The realization of holographic diffraction gratings in composite materials has been widely investigated in the past 20 years [1, 2]. It has been shown that devices based on holographic polymer dispersed liquid crystals (H-PDLC) have good diffraction efficiency. However those devices have some intrinsic drawbacks [3] because of the particular droplet structure of the nematic liquid crystal (NLC) formed in such gratings. Some years ago, a new kind of holographic diffraction grating made of polymer slices alternated with homogeneous films of NLC was realized, named Polymer Liquid Crystal Polymer Slices (POLICRYPS) [4]. The standard POLICRYPS grating writing process was performed on a stabilized setup [5]. A sharp and uniform morphology was obtained in such gratings and no droplet structure was observed [6]. To avoid the formation of the NLC droplets during the curing process, the syrup of photo-initiator-monomer-NLC mixture has to be heated up above the nematic-isotropic transition temperature of the NLC.

The POLICRYPS grating can be applied to high resolution display systems considering its high efficiency and low cost [7]. In this kind of applications, we are interested in the diffraction efficiency of the grating not only at normal incidence, i.e. the plane of incidence is perpendicular to the grating grooves, but also at conical incidence mount. In this case, the direction of the beam has to be specified not only by the polar angle θ with the normal but also by the azimuthal angle ϕ (see Fig. 1(a)). The azimuthal angle ϕ is the angle with the x -axis in Fig. 1(a).

In the past decades periodic gratings consisting of an anisotropic material have been studied by several researchers. The Coupled Wave Method for isotropic gratings [8] has been extended to anisotropic gratings by Rokushima et al. [9], Glytsis et al. [10], Mori et al. [11] and Montemezzani et al. [12]. The Chandezon method (C-method) has been applied to anisotropic gratings by Harris et al. [13]. Li [14] has extended his Fourier modal method (FMM) to anisotropic gratings as well. Li's FMM also allows conical incident angles.

Analytical methods often involve a simplification or approximation such that the formulae can be applied conveniently to a certain situation or configuration geometry and very often the calculation is restrained to extreme simple structures. Instead a versatile numerical method can handle more complex configurations and yield approximation solutions with sufficient accuracy. Therefore in our work a numerical code based on Finite Element Method (FEM) [15, 16] is employed to model the POLICRYPS gratings. The FEM is a flexible numerical method, because both periodic and non-periodic configuration and all kinds of materials can be modeled. In particular, anisotropic and inhomogeneous materials with arbitrary principle axes can be treated without problems. Compared to other methods, the extension to the anisotropic material is rather trivial. In this paper we present both simulation results and experimental measurements for both normal and conical incidence characterization of the POLICRYPS gratings. The Bragg transmission effect is also studied.

2. POLICRYPS gratings

The standard curing process to obtain a POLICRYPS grating has been discussed in Ref. [4]. An Ar^+ laser ($\lambda = 351$ nm) is used to obtain a UV-curing interference pattern. Both recording beams are TE polarized to maximize the intensity modulation. The recording angle θ_{record} is approximately 8.3° to achieve a grating pitch Λ of 1220 nm. The NLC weight concentration is 26% of the initial mixture, obtained by diluting NLC BL-001 (by Merck) with the pre-polymer system Norland Optical Adhesive NOA-61 [17]. In the curing process, first, a polymerization-driven redistribution of monomers and nematic components over the fringes of the interference pattern takes place. Second, a separation of the nematic phase follows which is in the dark regions of the interference pattern.

The dielectric permittivity modulations obtained for such a POLICRYPS grating is calculated accurately by a chemical-diffusion model [18]. In this model the concentration profile depends on two parameters G and B . The parameter G is proportional to the diffusion constant of the monomer and the other parameter B is proportional to the intensity of the curing pattern. To make POLICRYPS gratings, it requires that $G \ll 1$ and $B > 1$. The concentration of the polymer and the NLC are periodic functions of position in space, $v(\xi)$ and $\sigma(\xi)$ respectively with $\xi = (2\pi/\Lambda)x$. With the obtained concentration profiles, the index modulation profile in the x direction can be calculated by the following equation:

$$\varepsilon_x(\xi) = [\varepsilon_{\parallel} + (\varepsilon_{eff} - \varepsilon_{\parallel})\bar{v}(\xi)]\sigma(\xi) + \varepsilon_{pol}v(\xi), \quad (1)$$

where ε_{\parallel} and ε_{\perp} are the dielectric permittivity constants parallel and perpendicular to the director of the pure unaligned NLC, $\varepsilon_{eff} = (\varepsilon_{\parallel} + 2\varepsilon_{\perp})/3$ represents the effective dielectric constant of the LC and ε_{pol} is the dielectric permittivity constant of the polymer. In the above equations $\bar{v}(\xi) = v(\xi)/v_{max}$ represents the normalized polymer concentration. The obtained profile of the x-component is displayed in Fig. 1(b). Eq. 1 can be understood by considering some extreme cases for the concentrations of the involved chemical species. In those areas of the grating where only LC is present ($v(x) = 0$), we assume that LC molecules are oriented along the x -axis and TM-polarized probe light then experiences the dielectric constant:

$$\varepsilon_x(\xi) = \varepsilon_{\parallel}\sigma(\xi). \quad (2)$$

Another possibility is given when only polymer is present ($\sigma(\xi) = 0$). From Eq. 1 we see that:

$$\epsilon_x(\xi) = \epsilon_{pol}v(\xi). \quad (3)$$

In the points where the polymer concentration reaches a peak value ($\bar{v}(\xi) = 1$), we assume that some liquid crystal is dispersed in the polymer but its concentration is very low and hence its dielectric constant corresponds to the effective one ϵ_{eff} of the LC:

$$\epsilon_x(\xi) = \epsilon_{eff}\sigma(\xi) + \epsilon_{pol}(\xi)v(\xi). \quad (4)$$

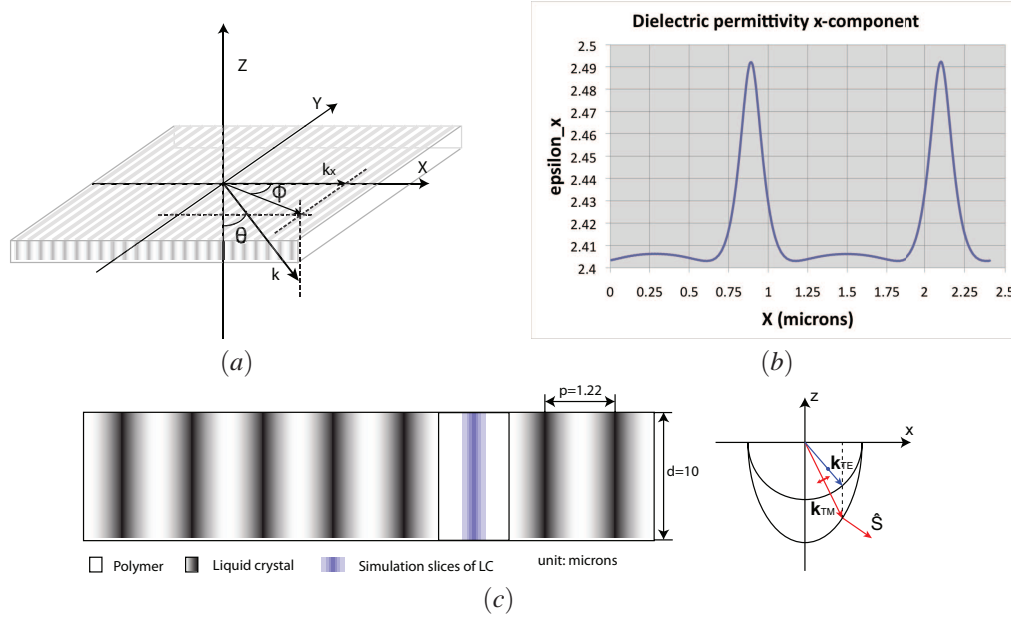


Fig. 1. (a) Coordinate system and angles θ and ϕ ; (b) Calculated x -component of the dielectric modulation; (c) Cross-section of the grating geometry and wave propagation direction of TM polarization. Respectively, \mathbf{k}_{TM} or \mathbf{k}_{TE} indicates the wave vector of the TM or TE polarization and \hat{S} is the unit vector along the Poynting vector of the TM polarized wave.

In the macro scale, the average director of the NLC is perpendicular to the walls of polymer slices, i.e. the optical axis of the NLC is along the x -axis, so that the parallel dielectric constant of the NLC is along the x -axis, i.e. $\epsilon_x = \epsilon_{\parallel}$ and the perpendicular dielectric constant of the NLC $\epsilon_y = \epsilon_z = \epsilon_{\perp}$ matches the dielectric constant of the polymer. Therefore the structure is functioning as a transmission grating for TM polarization of which the electric field can be expressed as:

$$\mathbf{E} = \begin{pmatrix} E_x \\ E_y \\ E_z \end{pmatrix} = A \begin{pmatrix} \cos \theta^i \\ 0 \\ \sin \theta^i \end{pmatrix}, \quad TM \text{ polarization} \quad (5)$$

where A is the amplitude. If the incident light is TE polarized, of which the electric field is:

$$\mathbf{E} = \begin{pmatrix} E_x \\ E_y \\ E_z \end{pmatrix} = A \begin{pmatrix} 0 \\ 1 \\ 0 \end{pmatrix}, \quad TE \text{ polarization} \quad (6)$$

it will not see the grating structure because of the match between the ordinary refractive index of the NLC ($n_o = \sqrt{\epsilon_{\perp}}$) and the refractive index of the polymer ($n_{pol} = \sqrt{\epsilon_{pol}}$) and will propagate through without being diffracted.

The wavefronts of the propagating waves in NLC are shown qualitatively in Fig. 1(c). The semi-circle is the wavefront of the TE polarization which senses the isotropic refractive index of NLC and the semi-ellipse is the wavefront of the TM polarization which sees the extraordinary refractive index of NLC. For the TM polarization the Poynting vector (energy flow) \hat{S} is not parallel to the direction of the wave vector, instead it is perpendicular to the surface of the wavefront as indicated in Fig. 1(c). When the optical axis of the NLC is along the x -axis as in our case, the Poynting vector always has the same sign in the z -component as the wave vector. This means that the TM polarization leaves the grating through the different surface from the incident wave, into the transmitted field. The TE and TM polarizations propagate out of the grating through the same surface. This illustrates the POLICRYPS as transmission gratings.

The geometry of the grating is shown in Fig. 1(c). The thickness of the grating is $10 \mu\text{m}$ and is sandwiched in a glass cell. In our simulation, a slice-structure is adapted to make a similar dielectric permittivity distribution as the real modulation profile shown in Fig. 1(b). From the center of the NLC concentration region to the interface with the polymer, 9 slices of region with gradually changing dielectric permittivities are defined and used. The dielectric permittivities and thickness of all slices are listed in Table 1. The refractive index of the polymer is about 1.515, of which accordingly the dielectric constant is 2.2952. In our simulation, for simplicity we assume there is only modulation in the x -component of the dielectric permittivity tensor and we take $\epsilon_y = \epsilon_z = 2.2952$.

	Thickness(nm)	ϵ_x
LC_1	46	2.492
LC_2	17	2.48
LC_3	12	2.47
LC_4	11	2.46
LC_5	18	2.45
LC_6	17	2.44
LC_7	23	2.43
LC_8	29	2.42
LC_9	215	2.41

Table 1. The dielectric permittivity of the vertical slices which parallel to the z -axis, into which the NLC has been divided to approximate the calculated profile shown in Fig. 1(b).

3. Methodology

3.1. Periodic gratings consisting of anisotropic material

We have studied anisotropic media that are translation invariant with respect to one direction in previous work [19]. It has been shown there that for a configuration consisting of anisotropic materials of which the dielectric permittivity $\underline{\epsilon}$ is invariant with respect to the y -coordinate, the Maxwell's equations can be reformulated as two coupled partial differential equations for the y -component of the electromagnetic field E_y and H_y only. In this work, the optical axis of the NLC in the POLICRYPS grating is perpendicular to the polymer walls and thus parallel to the

x -axis. The dielectric permittivity tensor of the NLC can be written as,

$$\underline{\underline{\epsilon}} = \begin{pmatrix} \epsilon_{xx} & 0 & 0 \\ 0 & \epsilon_{yy} & 0 \\ 0 & 0 & \epsilon_{zz} \end{pmatrix}, \quad (7)$$

with $\epsilon_{xx} = n_e^2 = \epsilon_{\parallel}$ and $\epsilon_{yy} = \epsilon_{zz} = n_o^2 = \epsilon_{\perp}$. Thus the equations from [19] can be reformulated as,

$$-i\omega\mu_0 H_y = i\nabla \cdot \left[\frac{1}{D} \mathcal{Q}^T \frac{\partial}{\partial x} \begin{pmatrix} k_y E_y \\ \omega_0 \mu_0 H_y \end{pmatrix} \right] + i\nabla \cdot \left[\frac{1}{D} \mathcal{M} \frac{\partial}{\partial z} \begin{pmatrix} k_y E_y \\ \omega \mu_0 H_y \end{pmatrix} \right], \quad (8)$$

$$i\omega\epsilon_0 \epsilon_{yy} E_y = -i \frac{k_y}{\omega \mu_0} \nabla \cdot \left[\frac{1}{D} \mathcal{N} \frac{\partial}{\partial x} \begin{pmatrix} k_y E_y \\ \omega \mu_0 H_y \end{pmatrix} \right] - i \frac{k_y}{\omega \mu_0} \nabla \cdot \left[\frac{1}{D} \mathcal{Q} \frac{\partial}{\partial z} \begin{pmatrix} k_y E_y \\ \omega \mu_0 H_y \end{pmatrix} \right] - \frac{i}{\omega \mu_0} \Delta E_y, \quad (9)$$

where ∇ is defined by,

$$\nabla = \begin{pmatrix} \partial/\partial x \\ \partial/\partial z \end{pmatrix}, \quad (10)$$

and

$$D = (\omega^2 \epsilon_0 \mu_0 \epsilon_{xx} - k_y^2)(\omega^2 \epsilon_0 \mu_0 \epsilon_{zz} - k_y^2), \quad (11)$$

$$\mathcal{N} = \begin{pmatrix} \omega^2 \epsilon_0 \mu_0 \epsilon_{zz} - k_y^2 & 0 \\ 0 & \omega^2 \epsilon_0 \mu_0 \epsilon_{xx} - k_y^2 \end{pmatrix}, \quad (12)$$

$$\mathcal{Q} = \mathcal{N} \begin{pmatrix} 0 & -1 \\ 1 & 0 \end{pmatrix} = \begin{pmatrix} 0 & -(\omega^2 \epsilon_0 \mu_0 \epsilon_{zz} - k_y^2) \\ \omega^2 \epsilon_0 \mu_0 \epsilon_{xx} - k_y^2 & 0 \end{pmatrix}. \quad (13)$$

$$\mathcal{M} = D \mathcal{N}^{-1} = \begin{pmatrix} \omega^2 \epsilon_0 \mu_0 \epsilon_{xx} - k_y^2 & 0 \\ 0 & \omega^2 \epsilon_0 \mu_0 \epsilon_{zz} - k_y^2 \end{pmatrix}, \quad (14)$$

Note that D is the determinant of matrix \mathcal{Q} . It is assumed here that $D \neq 0$. For the two polarization states TM and TE as defined in Section 2, in a general case, i.e. $k_y \neq 0$, the system is coupled. This means when the incident light is purely TM or TE polarized, the diffracted light will be elliptically polarized instead of preserving the linear polarization of the incident field. For $k_y = 0$ the plane of incidence is perpendicular to the grating structure, and then the TE and TM cases are uncoupled because for TE: $H_y = 0$ while for TM: $E_y = 0$.

In our work a numerical code based on Finite Element Method (FEM) [15, 16] is employed to perform the simulations. The FEM is a general numerical method for solving boundary value problems in mathematical physics. A computational domain in the (x, z) -plane is defined and is such that all nonplanar layers and all anisotropic layers are contained in its interior. The domain is truncated in the vertical direction by a Perfect Matched Layer (PML). In this computational domain, a boundary value problem for the vector Helmholtz equation for either the electric or magnetic field is formulated. The accuracy of the method has been tested for both normal incidence and conical incidence in our previous work.

We remark that the present model differs from the one described in [15, 16] on the numerical method used to solve the discretized linear system of equations. In [15, 16] an iterative method was used with approximate minimum fill-in (AMF) reordering and a preconditioner from ILU-PACK of Yousef Saad and Matthias Bollhoefer (see [20]). This preconditioning requires a lot of computation memory, in particular for three dimensional problems. In the present version of the code the sparse linear solver Pardiso [21, 22] is used. Due to this not only much less memory is needed, but also the computation time has been reduced drastically.

3.2. Bragg transmission grating

Consider a plane wave with wave vector \mathbf{k} incident on a periodic grating with pitch Λ , of which the grating vector is along the x -axis. The wave vector is given by,

$$\mathbf{k} = \begin{pmatrix} k_x \\ k_y \\ k_z \end{pmatrix} = k_o n^i \begin{pmatrix} \sin \theta^i \cos \phi^i \\ \sin \theta^i \sin \phi^i \\ \cos \theta^i \end{pmatrix}, \quad (15)$$

with $k_o = 2\pi/\lambda$, n^i is the refractive index of the incident medium and (θ^i, ϕ^i) are the angles of incidence. When the x -component of the wave vector satisfies the Bragg condition (see Fig. 2(a)),

$$-2k_x \cdot \Lambda = 2\pi \cdot m \quad (16)$$

where m is integer, constructive interference occurs, due to which a very high diffraction efficiency can be obtained in the m^{th} diffracted order. By substituting Eq. 15 in Eq. 16, we get

$$\sin \theta^i \cos \phi^i = -m \cdot \frac{\lambda}{2n^i \Lambda}. \quad (17)$$

If $m = -1$,

$$\sin \theta_B = \frac{\lambda}{2n^i \Lambda}, \quad \text{for } \phi^i = 0^\circ, \quad (18)$$

$$\sin \theta_B = \frac{\lambda}{2n^i \Lambda \cos \phi^i}, \quad \text{for } \phi^i \neq 0^\circ. \quad (19)$$

According to Eq. 19, the wave vector of the reading beam with incident angle (θ_B, ϕ^i) forms a cone in space as shown in Fig. 2(b)

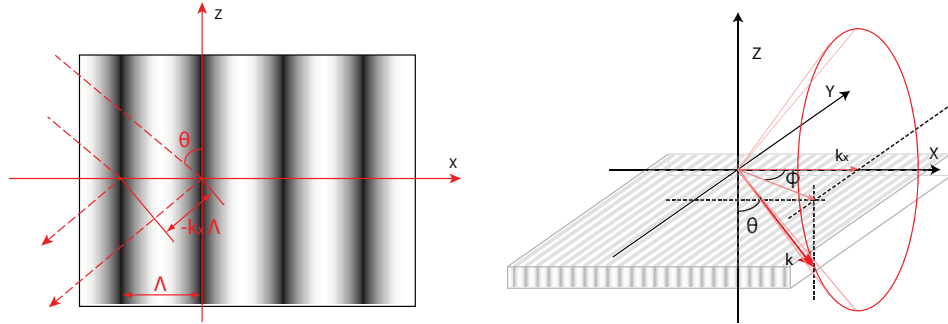


Fig. 2. (a)Bragg condition in (x, z) -plane; (b)Bragg condition in 3D space.

3.3. Experiment

A schematic diagram of the experimental set-up is shown in Fig. 3. Collimated laser light was used as light source. A polarizer was used to control the polarization of the reading beam. Two lasers were used in our experiment. One was a He-Ne Laser with wavelength of 633 nm and the other one, a diode laser with wavelength 532 nm. The intensity of the transmitted diffracted beams is measured by a photo-detector. A translation stage was designed such that the mounted grating sample can be tilted and rotated in three dimensions with any arbitrary angle (θ, ϕ) with high accuracy (in 0.1°) and stability. There are two operating angles α and β as shown in Fig.

3, which are different from the conventional definition of the combination of the polar angle θ and the azimuthal angle ϕ as shown in Fig. 1. The correlation between them can be expressed as,

$$\tan \alpha = \tan \theta \sin \phi, \quad (20)$$

$$\sin \beta = \sin \theta \cos \phi. \quad (21)$$

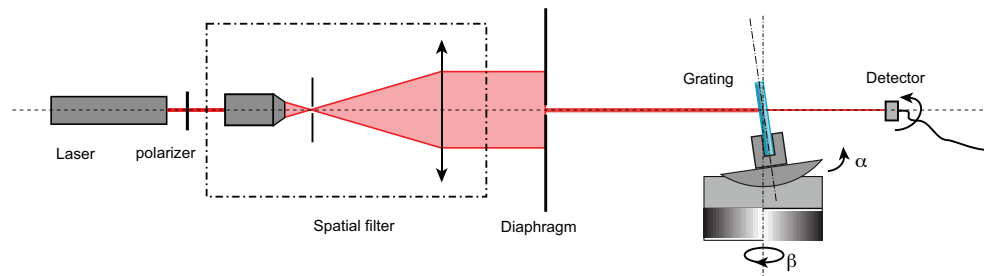


Fig. 3. Experimental set-up for both normal and conical incidence.

4. Results and discussion

4.1. Normal incidence

As has been discussed in Section 3.1, when the plane of incidence is perpendicular to the grating grooves, i.e. $\phi^i = 0^\circ$, the TE and TM polarization are uncoupled. The diffraction efficiency of the transmitted field for TM polarization was calculated and measured in this normal incidence mount. The efficiencies are plotted as function of the angle of incidence θ^i in Fig. 4. When the angle of incidence θ^i changes from 0° to 30° , there are three dominant diffracted orders for red light (633 nm), namely the $\pm 1^{st}$ (indicated as -1T and 1T in Fig. 4(a), and similar terms are used for other orders in the plots and we omit explaining each one when it occurs in the following text) and 0^{th} orders and for green light (532 nm), there are four dominant diffracted orders, namely the -2^{nd} , $\pm 1^{st}$ and 0^{th} orders. The sum of the intensity of the transmitted orders is defined as the total transmitted intensity I_{total} . The relative intensity of the diffracted orders is defined as the intensity of each order divided by the total intensity, $RI = I_{order}/I_{total}$.

The diffraction efficiencies are strongly dependent on the angle of incidence θ^i . The pitch of the POLICRYPS grating sample is 1220 nm. For red light with $\lambda = 633$ nm, the Bragg angle for the -1^{st} diffracted order is calculated with Eq. 18 and is equal to 15° , and for green light with $\lambda = 532$ nm, the Bragg angle for the -1^{st} diffracted order is 12.6° . For TM polarization a very high diffraction efficiency was observed when the angle of the incidence is equal to Bragg angle (θ_B). The high diffraction efficiency in the -1^{st} diffracted order at the Bragg angle is verified by the experimental measurements as shown in the Fig. 4. The narrow peak of the -1^{st} order shows that the POLICRYPS grating has a good angular selectivity. For the 633 nm reading wave, a very good agreement is obtained between the simulations and the measurements, by using the dielectric permittivity modulation profile shown in Fig. 1(b). For the green wave with $\lambda = 532$ nm, the refractive indices should be changed according to dispersion, but this could not be done accurately because we are dealing with a mixture of materials. It is the reason for the discrepancy at small and large angles of incidence for the green reading beam.

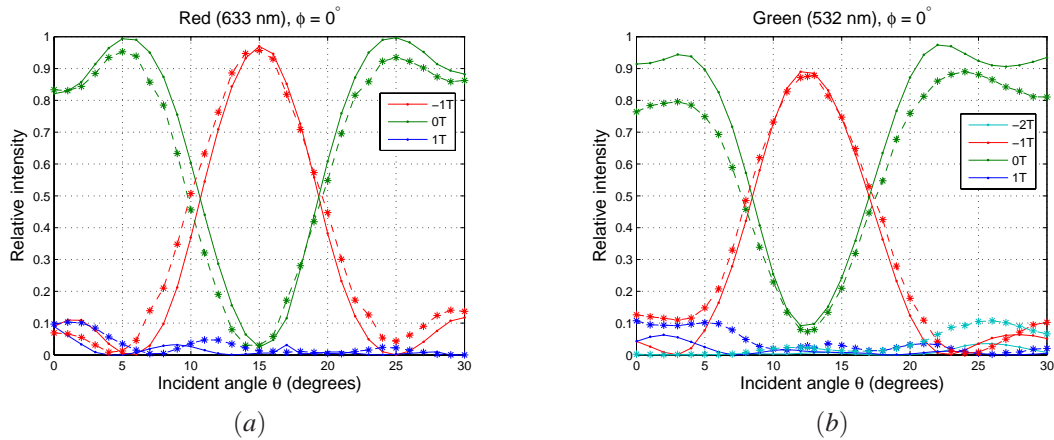


Fig. 4. The diffraction efficiency of TM polarization at normal incidence, i.e. $\phi^i = 0^\circ$ and $0^\circ \leq \theta^i \leq 30^\circ$ for (a) red light (633 nm) and (b) green light (532 nm). The star-dashed lines are experimental measurements and the dot-solid lines are calculations. In the legend, $-1T$ denotes the -1^{st} diffracted order of the transmitted field, etc.

4.2. Conical incidence

Conical incidence is of interest for the application to display systems [19, 23]. We have studied the diffraction efficiency of the POLICRYPS grating at conical incidence (the plane of incidence not perpendicular to the grating, i.e. $\phi \neq 0^\circ$) as shown in Fig. 5. The polarization of the

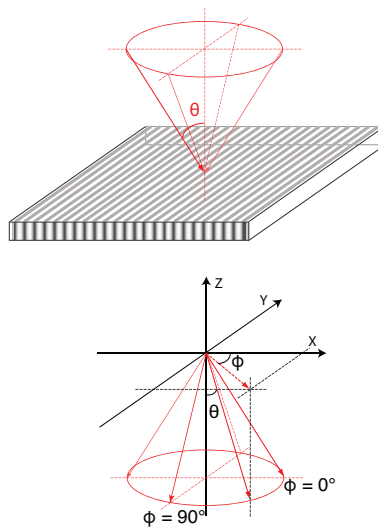


Fig. 5. Conical incidence configuration: the rays of incidence form a cone with respect to the normal of the POLICRYPS grating.

reading beam is TM. For fixed θ^i and varying ϕ^i in the range $0^\circ \leq \phi^i \leq 70^\circ$, the diffraction efficiency of the transmitted field was simulated and measured. The results are shown in Fig. 6. For red light (633 nm), $\theta^i = 15^\circ$ and for green light (532 nm), $\theta^i = 13^\circ$. When the plane of incidence is moving away from the perpendicular position to the grating structure, the Bragg

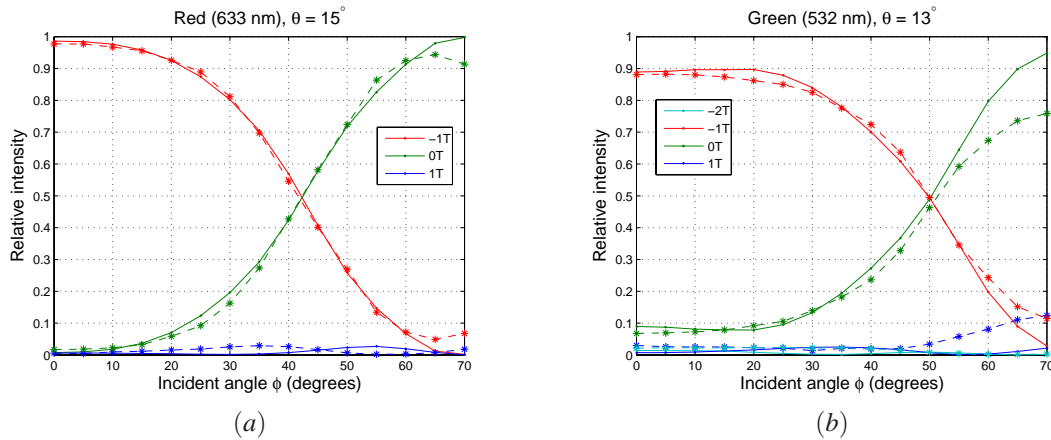


Fig. 6. The diffraction efficiency of TM polarization at conical incidence, for $0^\circ \leq \phi^i \leq 70^\circ$ and $\theta^i \doteq \theta_B$, for (a) red light (633 nm) $\theta^i = 15^\circ$ and for (b) green light (532 nm) $\theta^i = 13^\circ$. The star-dashed lines are experimental measurements and the dot-solid lines are simulations. In the legend, -1T denotes the -1^{st} diffracted order of the transmitted field, etc.

condition is not fulfilled anymore. The diffraction efficiency of the -1^{st} diffracted order decreases when ϕ^i is getting larger. This is predicted by the simulations shown in Fig. 6 (dot-solid lines in the figure) and confirmed by the experimental measurements (star-dashed lines). From the figure we can see that up to 20° the diffraction efficiency of the -1^{st} order is still quite high. This means that the POLICRYPS grating has a good tolerance range for the conical mount.

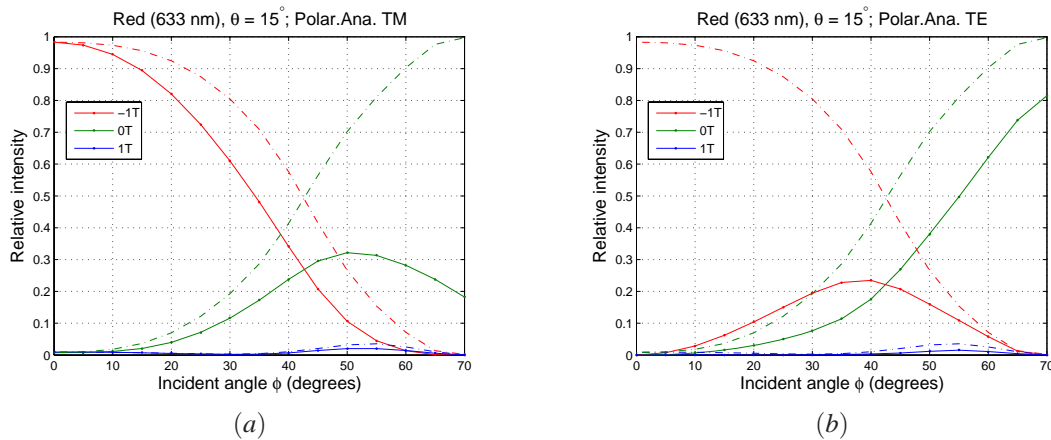


Fig. 7. Polarization analysis (based on simulation results) of the diffracted orders at the conical mount for 633 nm red light with (a) TM polarization analyzer and (b) TE polarization analyzer. The dash-dot lines are the same plots of the simulations results as in Fig. 6(a) and are included here as a reference for the two decomposed linear polarization in each order. In the legend, -1T denotes the -1^{st} diffracted order of the transmitted field, etc.

In Section 3.1, it has been shown that in a conical incidence mount, i.e. $k_y \neq 0$, the system of Eq. 8 and Eq. 9 are coupled and thus polarization states of the diffracted waves are different from that of the incidence wave. To analyze the polarization states of each diffracted order, the

electric field vector of each order is decomposed as two linear polarizations, TM and TE. The relative intensity for each linear polarization component is calculated based on the simulation results and is plotted in Fig. 7. It is easy to see the coupling between the two linear polarizations. When the azimuthal angle ϕ^i is small and the plane of incidence deviates from the normal incidence mount with a relatively small angle, the TM polarization dominates in the diffracted field. With the angle ϕ^i getting larger, TE polarization couples out in the diffracted orders. For some polarization sensitive applications, a polarization analyzer is necessary to be used with the POLICRYPS grating to remove the undesired polarization component in the transmission field.

4.3. 3D Bragg condition

As we discussed in Section 3.2, when the plane of incidence is not perpendicular to the grating structure, i.e. $\phi^i \neq 0^\circ$, a Bragg angle θ_B exists as function of ϕ^i . If the Bragg condition for the incident field is satisfied, a maximum diffraction efficiency can be obtained. To test this effect, TM-polarized light with wavelength 633 nm is used as reading beam. For the -1^{st} order, the Bragg angle θ_B is calculated for varying ϕ^i from 0° to 60° according to Eq. 19. For each ϕ^i , the incident angle θ^i is changed from $(\theta_B - 2^\circ)$ to $(\theta_B + 2^\circ)$. For each (θ^i, ϕ^i) the diffraction efficiency was calculated and measured. Then the angular distribution of the m^{th} diffracted order can be calculated for varying incident angles θ^i and ϕ^i from the following equations:

$$n^d \cos \phi^d \sin \theta^d = n^i \cos \phi^i \sin \theta^i + \frac{m\lambda}{\Lambda}, \quad (22)$$

$$n^d \sin \phi^d \sin \theta^d = n^i \sin \phi^i \sin \theta^i. \quad (23)$$

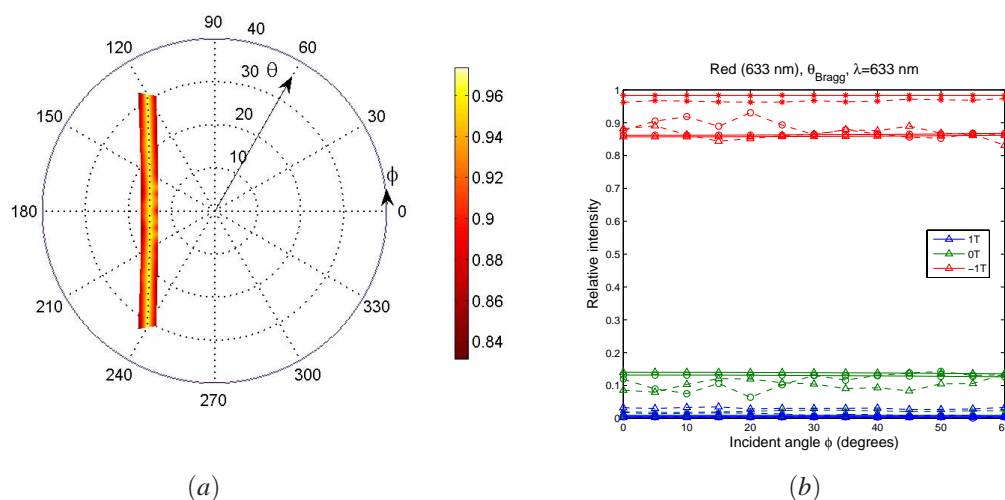


Fig. 8. (a) Measured angular distribution (θ^d, ϕ^d) of the diffraction efficiency of the -1^{st} diffracted order for the reading beam of 633 nm when the incident angles (θ^i, ϕ^i) follow the Bragg condition as discussed in Sec. 3.2. (b) Diffraction efficiency along the center (accordingly the incidence with Bragg angles marked with stars) and edges (accordingly incidence deviating from the Bragg condition marked with triangles (-2°) and with circles ($+2^\circ$)) of the ribbon in (a). The solid lines indicate simulated results, and the dashed lines experimental measurements.

The angular distribution of the diffraction efficiency of the transmitted field for the -1^{st} order is shown in Fig. 8. The transmitted field of the -1^{st} order spans a ribbon region. As is shown in the figure, the diffraction efficiency has a maximum at Bragg angle incidence (indicated by the dotted line in the center of the ribbon). The diffraction efficiencies at (θ_B, ϕ^i) (along the center dotted line in the ribbon of Fig. 8(a)) and at $(\theta_B \pm 2^\circ)$ (along edges of the ribbon) are shown as a function of the incident angle ϕ^i in Fig. 8(b). The curves show a uniform distribution of the diffraction efficiency at the corresponding Bragg incidence angles (θ_B, ϕ^i) .

5. Conclusions

POLICRYPS gratings offer very good optical properties because of their sharp and uniform morphology. A sample grating has been studied by using a rigorous model, as well as by experiments. A very good agreement is obtained between calculations and measurements. An experimental check of the grating efficiency at normal incidence shows a strong angular selectivity around the Bragg angle. By using a 633 nm reading beam, a maximum of about 95% in the diffraction efficiency at the Bragg angle is observed. When the reading beam is switched to 532 nm green light, a slightly dropped diffraction efficiency value evidences the wavelength dependence of diffraction performance of the POLICRYPS. A conical incidence characterization of the diffraction efficiency of the grating is performed for the first time. Results show a good tolerance range of conical tilting with the grating, indicating it is suitable for applications in e.g. display systems. A detailed characterization has shown that a uniform high diffraction efficiency can be achieved by moving the incident angles along the Bragg angle of incidence in 3D space.

Acknowledgments

This research is part of STW - Dutch Technology Foundation project DOE. 6823.